Dynamic Changes in Land Cover and Its Effect on Urban Heat Islands

Linxue Tian, Jun Yang, and Cui Jin

***Abstract*—Several studies have demonstrated that the urban heat island (UHI) impact is significantly influenced by changes in urban land cover (LC). In this study, we examined the dynamic change in LC in Shijiazhuang city and its impact on UHI intensity using multisource data, including landsat and LC data. The results showed that 1) the 15-year span exhibited a substantial growth in built-up area from 14.541% to 19.718%, whereas cropland and grassland dropped by 3.342% and 3.625%, respectively. 2) The mean land surface temperature (LST) in the study area increased significantly. From a point-to-plane distribution, the high-temperature zone (>32 °C) grew, and the direction of growth was consistent with urbanization. 3) The average temperature of the barren areas was the highest, followed by the built-up areas. 4) The normalized difference vegetation index and LST have a strong negative association, showing that LST rises with vegetation loss. Our research results provide a scientific basis for deeper understanding of the mechanisms underlying UHI creation, as well as for developing logical land use strategies and evaluating the effects of urbanization on local climates.**

***Index Terms*—Land cover (LC), normalized difference vegetation index (NDVI), urban heat island (UHI), urbanization.**

I. Introduction

URBANIZATION is a significant change in human society, an irreversible development trend, and the only way for human society to modernize [1]. Urbanization drives urban development, changes in production and the way of life, and leads to a rapid increase in greenhouse gas and pollutant emissions. It also drives changes in land cover (LC) types and spatial patterns, mainly by the replacement of vegetation cover and soil with concrete and asphalt surfaces [2], [3]. The optical characteristics of urban surfaces have undergone significant transformations. These impervious LC classes, often referred to as infrastructure, have a major influence on land surface temperature (LST) [4]. In recent years, LC changes associated with urbanization have been shown to have significant climatic impacts [5]. Urban areas exhibit higher temperatures compared to the adjacent nonurban areas, a phenomenon known as urban heat islands (UHI) [6], [7]. UHI can negatively impact climate, plants, air, and water in a city [8], [9], [10], [11], [12], [13]. For urban dwellers, this further exacerbates the heat stress induced by heat waves, which can have deleterious consequences on human health and even increase mortality and morbidity [14].

A part of the UHI study monitored and recorded the temperature of the city and its surrounding areas in real time by deploying temperature observation points using meteorological sites. Through the statistical analysis of long-term observational data, the characteristics of the UHI, as well as the trend of change, can be derived [15]. The other part is understood through remote sensing data [16], [17], [18], which uses remote sensing technologies, such as satellites and airplanes, to acquire temperature information of cities and their environs. Through a comparative analysis of the temperature distribution of different regions, the formation and evolution of the UHI can be revealed [19]. It involves the related content of hyperspectral image processing, hyperspectral images contain rich information [20], and has broad application prospects in environmental monitoring, urban survey, mineral exploration, military investigation, and many other aspects. Traditional target detection methods require prior information about the target, which is often difficult for researchers to obtain in practice. Therefore, how to achieve target detection without prior information is the focus of current research. This kind of object detection algorithm without prior knowledge is called anomaly detection. A new study treats anomaly detection as a frequency-domain analysis problem, which is represented by phase reconstruction [21]. Compared with the existing anomaly detection methods, this method has remarkable detection performance and time efficiency. Some scholars also use a new perspective of information theory to transform system entropy into a quantitative measure of pixel anomaly significance [22].

Remote sensing technology has facilitated the acquisition of LST data, which is more readily accessible compared with temperature data obtained from meteorological stations and has the advantages of large coverage, good time synchronization, and spatial continuity. Many sensors are currently employed for LST inversion, such as the AVHRR data from NOAA satellites

Manuscript received 26 September 2023; revised 21 November 2023; accepted 7 December 2023. Date of publication 14 December 2023; date of current version 8 January 2024. This work was supported in part by the National Natural Science Foundation of China under Grant 41771178 and Grant 42030409, in part by the Basic Scientific Research Project (Key Project) of the Education Department of Liaoning Province under Grant LJKZ0964, in part by the Fundamental Research Funds for the Central Universities under Grant N2111003, and in part by the Natural Science Foundation of Guizhou Province under Grant (2019)1150. *(Corresponding authors: Jun Yang; Cui Jin.)*

Linxue Tian is with the Liaoning Normal University, Dalian 116029, China (e-mail: tianlin1617@163.com).

Jun Yang was with the Human Settlements Research Center, Liaoning Normal University, Dalian 116029, China. He is now with the Jangho Architecture College, Northeastern University, Shenyang 110169, China (e-mail: yangjun8@mail.neu.edu.cn).

Cui Jin is with the Human Settlements Research Center, Liaoning Normal University, Dalian 116029, China (e-mail: cuijin@lnnu.edu.cn).

This article has supplementary downloadable material available at https://doi.org/10.1109/JSTARS.2023.3342988, provided by the authors.

Digital Object Identifier 10.1109/JSTARS.2023.3342988

[23], [24], [25], [26] and MODIS from Terra/Aqua satellites data [27], [28], [29], [30], [31], which are more suitable for large-scale studies owing to their insufficient resolution [32]. Landsat series data with medium resolution can provide wider coverage and richer information on surface features, which can characterize the urban surface thermal environment and are more suitable for the inversion of LST in mesoscale areas [33]. The Landsat series is extensively utilized due to the convenient availability of data. As an illustration, Yu et al. [34] compared three LST inversions using Landsat8 data.

Various factors contribute to the fluctuations in LST, including solar radiation, climate and weather, soil and vegetation, and ocean effects. Soil and vegetation play important roles in regulating the LST. Therefore, the LC mode has an important influence on changes in LST [35]. Previous studies have used various methods, including the examination of the diurnal temperature range [36], land-use change trajectories [37], temperature vegetation index space [38], and UHI ratio index [39] to study the relationship between LC transition and surface temperature. Many studies have focused on a single time [40], different seasons [41], [42], [43] or different years [44]. In addition, the effects of LC on LST in different climatic zones were analyzed. For instance, Xin et al. [45] came at the conclusion that LST varied significantly for each land type in different climate zones. Geng et al. [46] conducted a comparative analysis of urban parks situated in distinct climate zones and found that the cooling effects were different. These studies have successfully demonstrated the contribution of urban expansion to UHIs. However, it is difficult to use these methods to gain insight into how divergent spatial patterns of urban development affect UHIs. Understanding which types of urban sprawl enhance or reduce the impact on UHIs helps develop effective strategies for heat island control.

For reference in urban planning, this study quantified the LST changes brought on by various LC changes by analyzing the spatiotemporal characteristics of LC and LST in Shijiazhuang city from 2004 to 2019 using multisource data, including Landsat and LC data. It also looked at the correlation between LC changes and LST distribution.

II. Materials

A. Study Area

One of the most significant cities in Beijing–Tianjin–Hebei is Shijiazhuang, which is located in the central region of China. The geographical coordinates of the area lie within the range of 37°27′–38°47′ N and 113°30′–115°20′ E in the central and southern parts of North China and Hebei Province. Spanning the Taihang mountains and North China plain, eight districts and fourteen counties have jurisdiction over this city; the terrain is low in the southeast and high in the northwest, the gap is large, and the landform is intricate. The city is situated in proximity to the Bohai Sea and experiences a temperate monsoon environment. Solar radiation is marked by seasonal fluctuations, with high and low atmospheric pressure on the ground frequently occurring; the four seasons clearly distinguished, with summer being characterized by high temperatures and abundant rainfall, winter is characterized by cold temperatures and limited precipitation. Since the 1990s, the region has experienced rapid urbanization, extensive development of land for cities, and an influx of people into urban centers (Fig. 1).

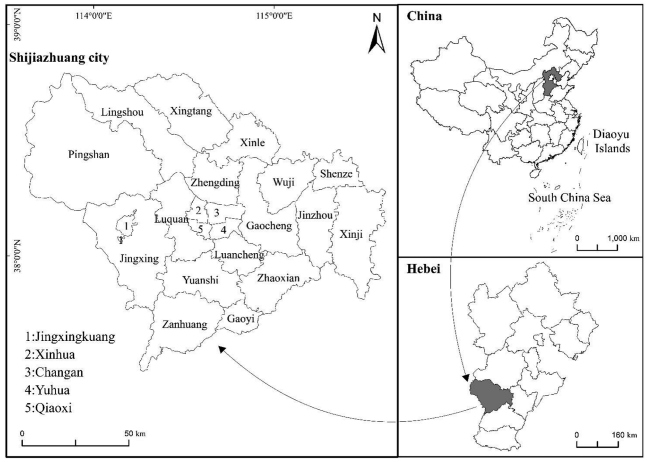

Fig. 1. Location of the study area (Shijiazhuang, China).

TABLE I
LC Types and Their Descriptions

Classification	Description
Cropland	Agricultural land (where used for farming)
Forest	Orchards, trees, shrubs, etc.
Grassland	Grasses, flowering plants, and light plants
Water	Lakes, rivers, wetlands, etc.
Barren	Waste land and unused land
Built-up area	Mixed Urban, residential, etc.

TABLE II
Data Sources and Descriptions

Satellite	Sensor	Orbiter	Date	Resolution
Landsat5	TM	124/33,124/34	2004.08.30 2010.08.15	30m (Band-6 excepted)
Landsat8	OLI/TIRS		2015.08.13 2019.07.23	30m (Band-8 excepted)

B. Data

For the purposes of this study, the dataset utilized was obtained from "the 30 m annual LC datasets and its dynamics in China from 1985 to 2022," which has the biggest advantage of 30 m annual LC classification results for more than 30 years [44]. It has a higher time resolution than other products, and the dataset can be downloaded for free at https://doi.org/10.5281/zenodo.8176941. We reclassified the LC into six categories based on the geographic and climatic characteristics of Shijiazhuang city, i.e., 1) cropland, 2) forest, 3) grassland, 4) water, 5) barren, and 6) built-up area (see Table I).

This study used Landsat5 thematic maps (TM) (2004 and 2010) and Landsat8 operational land images (OLI) (2015 and 2019). This information was provided by the United States Geological Survey. All photos were captured throughout the summer to better expose the peculiarities of the UHI distribution (see Table II, with <5% cloudiness in the study area, and processed

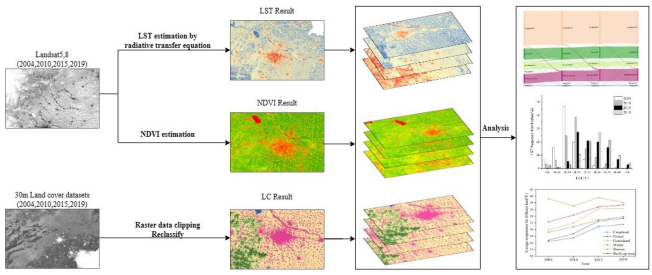

Fig. 2. Research framework and data processing.

using ENVI for radiometric calibration, atmospheric correction, and image cropping.

III. Methods

In this study, we integrated multisource data with landsat imagery for LC classification, LST inversion, normalized difference vegetation index (NDVI) attribute mapping, and correlation analysis among LC, LST, and NDVI. The overall framework and main data processing methods are shown in Fig. 2.

A. Inversion of LST

In this study, we used RTE, a conventional technique rooted in atmospheric radiative transfer modeling. Although the steps for inverting the surface temperature using this method are complex, it is more accurate compared with other methods and can be applied to any thermal infrared band, where the expression for the brightness value of thermal infrared radiation L_λ that the satellite sensor picked up can be expressed as

$$L_\lambda = [\varepsilon B(T_s) + (1-\varepsilon) L\downarrow]\tau + L\uparrow \tag{1}$$

where ε is the surface specific emissivity, T_s is the true surface temperature K, $B(T_s)$ is the blackbody radiant luminance, and τ is the atmospheric transmittance in the thermal infrared band, obtained from https://atmcorr.gsfc.nasa.gov/. The radiant brightness $B(T_s)$ of a blackbody at temperature T in the thermal infrared band is defined as follows:

$$B(T_S) = [L_\lambda - L\uparrow - \tau(1-\varepsilon) L\downarrow]/\tau\varepsilon \tag{2}$$

where the true surface temperature T_s can be obtained as a function of Planck's formula, as follows:

$$T_s = K_2/\ln(K_1/B(T_s)+1). \tag{3}$$

For the different sensors, the values of K_1 and K_2 were different because the data sources selected for this experiment were Landsat5 and Landtsat8 remote sensing images of Shijiazhuang, and their corresponding sensors were TM and OLI/TIRS, respectively. Thus, for TM data, K_1 =6 07.76 $W/m^2 \cdot \mu m \cdot sr$ and K_2 = 1260.56 K; for OLI/TIRS data, K_1 = 774.89 $W/m^2 \cdot \mu m \cdot sr$ and K_2=1321.08 K.

B. LC Dynamic Index

To accurately quantify the rate of change of LC types, such as built-up areas, in different time periods, this study selected a single LC dynamic attitude, K. This indicator is used to characterize the quantitative changes of a certain LC type in a certain time frame and is a more ideal research tool to analyze the overall average rate of change of a single LC type; its mathematical expression is

$$K = \frac{U_{bi} - U_{ai}}{U_{ai}} \times \frac{1}{T} \times 100\% \tag{4}$$

where K denotes the rate of change in the LC type per unit time, U_{ai} denotes the area of LC type i at the beginning of the study, U_{bi} denotes the area of LC type i at the end of the study, and T denotes the length of the cycle to be set for the study (in years).

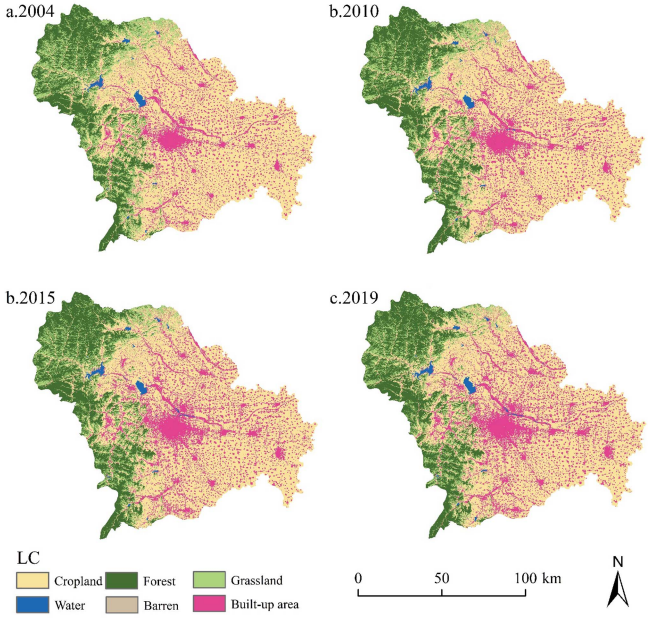

Fig. 3. Results of LC classification.

C. Retrieval of NDVI

The efficacy of NDVI in utilizing satellite technology for the evaluation and surveillance of worldwide vegetation coverage has been firmly proven during the past twenty years, making it the most widely used index [45], [46]. NDVI is often used as a metric to assess land characteristics, specifically to establish the correlation between soil greenness and LST. [47]. The value was expressed as follows:

$$NDVI = \frac{NIR - R}{NIR + R} \tag{5}$$

where NIR is the reflection value of the near-infrared band and R is the reflection value of the red band.

When the NDVI value is close to -1, the visible light is highly reflective. A value of 0 means that NIR and R are approximately equal, and there is rock or bare soil; a positive value means that there is vegetation cover, such as forests and farmland.

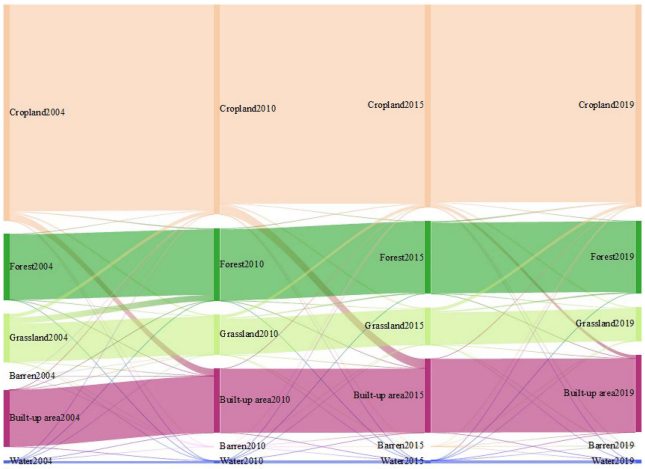

Fig. 4. Changes in the proportion of different LC types from 2004 to 2019.

IV. Results and Analysis

A. LC Classification and Change Analysis

Figs. 3 and 4 and Table VII of the Appenix show that, a marked increase in built-up area (5.177%), a significant decreasve in the proportion of cropland (−3.342%) and grassland (−3.625%), an increase in the proportion of forest (1.605%), and the proportions of water (0.195%) and barren (−0.010%) remained nearly constant. According to the data shown in Table VIII, of the Appenix the amount of land covered by built-up areas expanded by 260.995 km^2 between the years of 2004 and 2010, with the majority of this expansion occurring in Xinhua, Chang'an, Yuhua, Qiaoxi, and Luquan districts, with the main contributors in this period being cropland (96.2%) and grassland (3.5%). Between 2010 and 2015, there was a notable rise in the extent of built-up areas, amounting to 347.961 km^2, with changes primarily concentrated in Xinhua, Chang'an, Yuhua, Qiaoxi, Luquan, Gaocheng, and Luancheng districts. The main contributors during this period were croplands (97.5%) and grasslands (2.9%). Between 2015 and 2019, the amount of built-up area grew by 119.450 km^2, and we can see that several districts where the main changes occurred before changed insignificantly and that all administrative districts witnessed a slight augmentation in built-up area during this period. The main contributors in this period continue to be cropland (98.4%) and grasslands (4.8%). Overall, from 2004 to 2019, the built-up area amounting to a total increase of 728.406 km^2, of which cropland contributed 97.2%. Grasslands and forests contributed 3.5% and 1.1%, respectively, whereas other LC types were negligible. Urbanization in the primary urban region of Shijiazhuang occurs at the expense of cropland, with the fastest growth in the Yuhua and Qiaoxi districts, which also indicates that although urbanization in Shijiazhuang occurs in all directions, though it is still primarily from northwest to southeast.

Table III reveals that from 2004 to 2019, the LC types in the region showed the change characteristics of several types increasing and others decreasing; the main increasing types were forest, water, and built-up areas, with growth rates of 0.63%, 1.97%, and 2.37%, respectively. In terms of the speed about change, the built-up area had the largest growth rate, and during 2010–2015, there was a notable increase in the built-up area, with a K value as high as 3.02%, followed by water, with a growth rate of 1.97%; and the direction of change of the K value remained consistent from 2004–2019, with a K value of 4.26% during 2015–2019. Forest had the smallest increase with a K value of 0.63%, except for 2015–2019, when the increase in forest was negative. The rate of increase was 1.62% and 0.02% from the beginning of 2004 to 2015, and the K value showed a decreasing trend during 2010–2015 compared with the previous period.

TABLE III
Dynamic Change of Single LC in the Study Area From 2004 to 2019

LC	Cropland	Forest	Grassland	Water	Barren	Built-up area
K2004-2010	-0.43%	1.62%	-2.81%	0.19%	0.96%	2.13%
K2010-2015	-0.67%	0.02%	-1.42%	1.87%	-8.96%	3.02%
K2015-2019	-0.05%	-0.07%	-2.15%	4.26%	-4.31%	1.12%
K2004-2019	-0.40%	0.63%	-1.96%	1.97%	-3.45%	2.37%

The K values of cropland, grassland, and barren land have the same direction of change and are all negative, −0.40%, −1.96%, and −3.45%, respectively, which fully indicates that the land for these three types of utilization has been shrinking in the past 15 years. Among them, barren land had the largest decrease, with a K value of −3.45%, and the rate of change was negative at every stage from 2010, with a K value of −8.96% and −4.31%, respectively. The negative growth of grassland is only second to that of barren land, with a K value of −1.96%, and the area of grassland is in a state of shrinking, which is an important signal for Shijiazhuang city, and the utilization and protection of grassland resources require attention. Cropland showed the smallest reduction with a K value of −0.40%, with K values of −0.43%, −0.67%, and −0.05% for each stage.

B. Relationship Between LST and Changes in LC Classification

Fig. 5 shows the variation in how the LST was spread out in space in Shijiazhuang changed over the study time. The classification system comprises nine distinct categories, each delineated by specific temperature ranges. The low-temperature zone is defined as temperatures below 26 °C, while the high-temperature zone encompasses temperatures over 32 °C. No significant UHI phenomenon was observed in 2004. By 2010, the high-temperature areas on the map began to spread, mainly representing industrial areas, densely populated areas, open grounds, and commercial areas. It was cooler in areas with numerous plants. As the area increased, the temperature at the center gradually decreased. In 2015, many high-temperature areas were distributed on the map. In addition, previously dispersed hotspots exhibited a steady expansion and connection, resulting in a transition from a point to a plane distribution. In 2019, the hot regions expanded further, a high-temperature planar distribution was fully formed, and more hot regions were

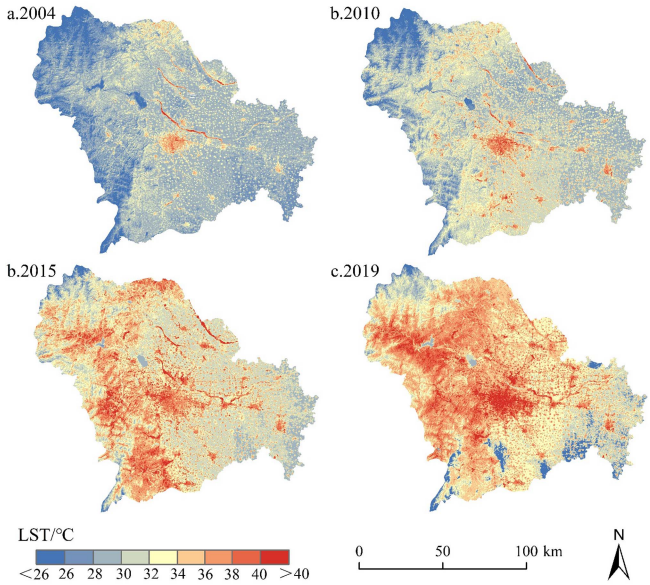

Fig. 5. LST distribution in Shijiazhuang.

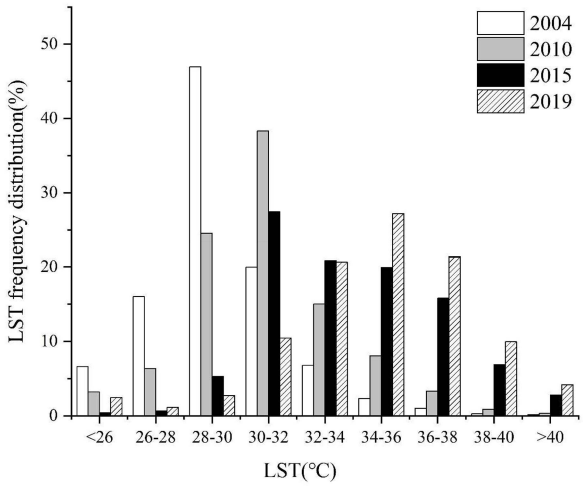

Fig. 6. LST distribution in different years.

created owing to the change in LC from cropland and grassland to built-up areas.

The LST of Shijiazhuang has increased significantly. In 2004, the temperature distribution was between 28 °C and 30 °C, the highest was 47.01 °C and the lowest was 15.88 °C. In 2019, the temperature distribution was between 34 °C and 36 °C, the amplitude of the change increased significantly; the highest was 63.82 °C and the lowest was 9.22 °C. In 2004, the LST was predominantly <30 °C, and 28 °C–30 °C accounted for 46.94% of the total; by 2010, the LST was concentrated between 30 °C–32 °C, accounting for 38.31%; by 2015, the LST range of the concentration distribution did not change, but the percentage of area >32 °C was as high as 66.27%; by 2019, the LST concentration distribution was 36 °C–38 °C (27.18%), the percentage of >32 °C reached 83.23%, and the percentage of low LST decreased to 2.48% (<26 °C) and 3.83% (26–30 °C). The histogram (see Fig. 6) illustrates the variations in the

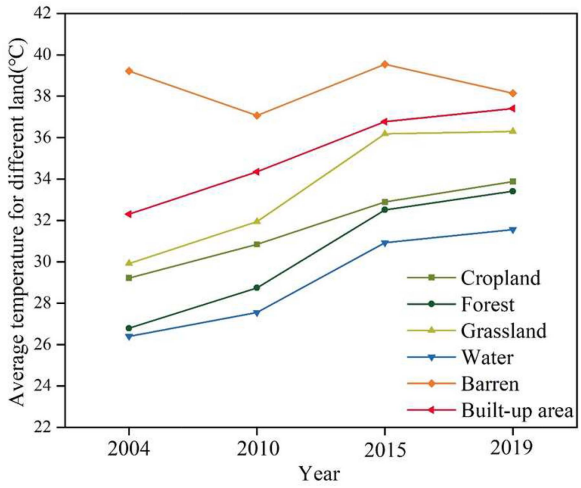

Fig. 7. Mean temperature of different LC in different years.

temperature profile. During the 2004–2019 study period, the LST distribution was homogeneous, with a gradual shift in the distribution intervals toward the high-temperature zone.

The minimum, maximum, and mean LSTs as well as the standard deviation (STDEV) values for each LC were computed to explore their influence on the LST (see Appendix Table IX). The total STDEV was the smallest for cropland and water, that is, because of their relatively simple nature and small temperature variations. However, the built-up areas have a larger STDEV because of the urban structure, layout, and differences in building materials. Forests and grasslands also have high STDEV because they include shrubs and trees, and therefore, a wide range of temperatures. The STDEV for barren land was also high because of the complex nature of unutilized land and, therefore, the wide range of temperatures.

Fig. 7 illustrates the observed increase in average temperature within the built-up area, which ranks second in terms of temperature rise, following the barren area. The overall change in croplands showed a steady upward trend, and the trends in grasslands and forests were similar in magnitude, likely because of differences in plant growth. Overall, the LST increased annually for all types, which can be elucidated by the enhanced UHI effect. Water and forests are the most effective ways to lessen the effects of a heat island. Therefore, water resources and forests should be protected. The LST of barren had a higher value compared with other types of LC; therefore, the management of barren land should be strengthened to avoid increasing temperatures due to the increase in barren land as a result of degradation of cropland and forests.

In order to further study the relationship between LST and LC change, we setup 2, 5, and 10 km buffer zones in the four main urban areas of the study area (see Fig. 8), which contain different types of LC. From 2004 to 2019, the proportion of built-up area in the 2 km buffer zone increased from 37.47% to 54.91%, the 5 km buffer zone from 31.52% to 48.22%, and the 10 km buffer zone from 22.22% to 32.07%. During the period of 15 years, with the increase of buffer area and the change of LC type, the change of LST was also large, with an overall increase of 6 °C

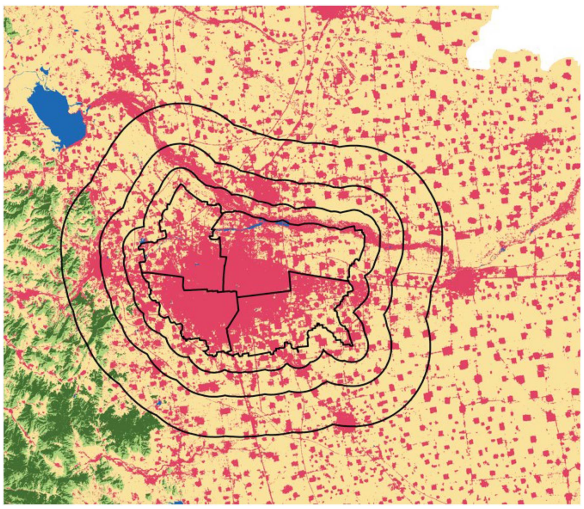

Fig. 8. Buffer zone in main urban area.

TABLE IV
LST IN DIFFERENT BUFFER ZONES

LST(°C) / Year	2 km	5 km	10 km
2004	31.14	30.71	30.02
2010	32.96	32.56	31.80
2015	35.48	35.27	34.25
2019	37.33	36.87	36.06

TABLE V
AVERAGE NDVI FOR DIFFERENT LC TYPES

Year	Cropland	Forest	Grassland	Water	Barren	Built-up area
2004	0.663	0.692	0.573	-0.149	0.184	0.364
2010	0.722	0.730	0.608	-0.158	0.145	0.378
2015	0.656	0.764	0.605	-0.140	0.135	0.338
2019	0.665	0.783	0.644	-0.282	0.170	0.377

(see Table IV). It can be found that the rapid expansion of the city in these years led to the temperature increase of the city and its surrounding areas is very significant.

C. Relationship Between LST and NDVI

As given in Table V, the NDVI was highest in forests and lowest in water. Built-up areas are larger than barren areas because barren areas are not covered with any material and built-up areas have artificial plantations. Fig. 9 shows the NDVI distribution in the region from −1 to 1. From 2004–2019, the green areas continued to decline, and the red areas continued to increase; with the continuous expansion of the city, it extended from the city's core to its outside regions.

To study their relationship, data pertaining to both variables were from different LC, and Pearson correlation coefficients were calculated (see Table VI). The maximum correlation coefficient was 0.980 (water in 2015), which was also the only one showing a positive correlation. The reason for this phenomenon is that water present negative NDVI values and lower LST;

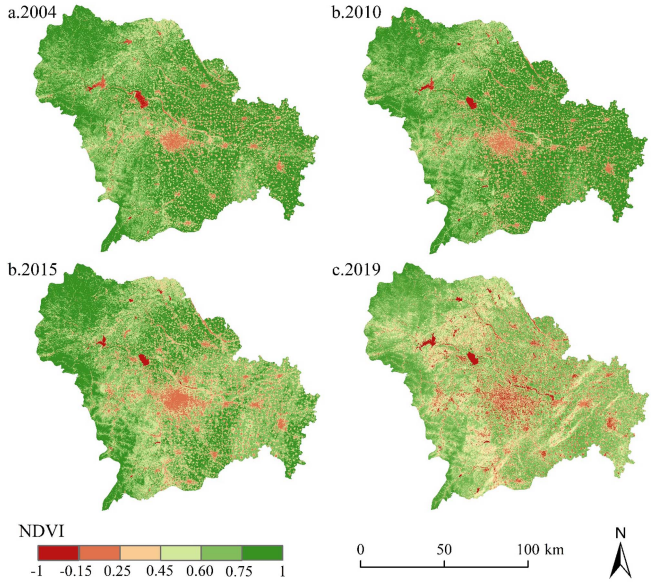

Fig. 9. NDVI map in each year. (Jenks natural breaks classification).

TABLE VI
NDVI AND LST AT DIFFERENT LC BY THE PEARSON COEFFICIENT

LC	2004	2010	2015	2019
Cropland	-0.583**	-0.806**	-0.760**	-0.621**
Forest	-0.512**	0.224*	-0.590**	-0.584**
Grassland	-0.672**	-0.499**	-0.582**	-0.510**
Water	0.398	0.315	0.980**	0.823**
Barren	-0.045	0.248	-0.601**	-0.406**
Built-up area	-0.021	-0.435**	-0.595**	-0.308**

Note: * p<0.05 ** p<0.01

therefore, they are less affected by vegetation. Cropland (−0.806 in 2010), forest (−0.590 in 2015), and grassland (−0.672 in 2004) had stronger negative correlation coefficients, whereas built-up area (−0.021 in 2004) had weaker negative correlation coefficients.

These results suggest a strong correlation between the NDVI and LST. There exists an inverse relationship between them, whereby an increase in NDVI corresponds to a decrease in LST. Several things are to blame for this, such as evaporation and transpiration, which can remove heat and thus reduce surface temperatures. [48].

V. DISCUSSION

A. Shijiazhuang Urban Heat Island

This study combined satellite image data and LC data to determine that the changes in LST distribution in Shijiazhuang city are due to the influence of the different nature of LC. The overall relationship between the direction of LST increase and that of urbanization is consistent with the findings of most studies [49], [50], [51], [52], and the evolution of the spatial distribution of the UHI effect is closely linked to urban expansion. However, a few studies have found that urbanization produces a cold island effect, and this discrepancy is primarily caused by the arid conditions affecting the study areas [53], [54], [55]. In addition,

TABLE VII
DISTRIBUTION CHANGES OF EACH LC TYPE DURING THE STUDY PERIOD

LC / Year	Cropland		Forest		Grassland		Water		Barren		Built-up area	
	km²	%	km²	%	km²	%	km²	%	km²	%	km²	%
2004	7817.176	55.557	2376.492	16.890	1735.159	12.332	93.083	0.662	2.662	0.019	2046.043	14.541
2010	7616.729	54.132	2607.162	18.529	1442.714	10.253	94.156	0.669	2.816	0.020	2307.038	16.396
2015	7360.927	52.314	2609.642	18.547	1340.516	9.527	102.977	0.732	1.554	0.011	2654.999	18.869
2019	7346.919	52.215	2602.319	18.495	1225.110	8.707	120.533	0.857	1.286	0.009	2774.449	19.718
Overall	-470.257	-3.342	+225.837	+1.605	-510.049	-3.625	+27.450	+0.195	-1.376	-0.010	+728.406	+5.177

TABLE VIII
TRANSFER MATRIX OF LC IN SHIJIAZHUANG (2004–2019)

Unit:km²	2010						
2004	Cropland	Forest	Grassland	Water	Barren	Built-up area	Overall
Cropland	7465.986	39.790	53.006	7.315	0.076	251.003	7817.176
Forest	12.815	2350.473	10.772	0.006	0	2.426	2376.492
Grassland	128.444	216.809	1378.810	0.236	1.522	9.338	1735.159
Water	8.780	0.088	0.008	83.073	0.020	1.114	93.083
Barren	0.511	0	0.116	0	1.199	0.836	2.662
Built-up area	0.192	0.002	0.001	3.526	0	2042.322	2046.043
Overall	7616.729	2607.162	1442.714	94.156	2.816	2307.038	14070.615

Unit:km²	2015						
2010	Cropland	Forest	Grassland	Water	Barren	Built-up area	Overall
Cropland	7216.657	10.795	45.266	4.832	0.004	339.175	7616.729
Forest	30.822	2559.070	13.636	0.003	0	3.632	2607.162
Grassland	110.827	39.775	1281.290	0.117	0.466	10.238	1442.714
Water	2.445	0.003	0.012	90.921	0	0.776	94.156
Barren	0.135	0	0.312	0.011	1.084	1.274	2.816
Built-up area	0.040	0	0	7.094	0	2299.904	2307.038
Overall	7360.927	2609.642	1340.516	102.977	1.554	2654.999	14070.615

Unit:km²	2019						
2015	Cropland	Forest	Grassland	Water	Barren	Built-up area	Overall
Cropland	7173.447	12.893	43.284	13.758	0.003	117.542	7360.927
Forest	49.298	2540.885	17.393	0	0	2.066	2609.642
Grassland	121.308	48.539	1164.306	0.146	0.483	5.734	1340.516
Water	2.639	0.002	0.002	99.933	0.003	0.399	102.977
Barren	0.084	0	0.125	0.018	0.797	0.530	1.554
Built-up area	0.142	0	0	6.678	0	2648.179	2654.999
Overall	7346.919	2602.319	1225.110	120.533	1.286	2774.449	14070.615

NDVI showed a negative correlation with UHI, which agrees with other studies [56], [57]. This shows that if one wants to mitigate the UHI effect, one can increase the area of green spaces appropriately.

Through the development history of Shijiazhuang city from 2004 to 2019, the urbanization rate of Shijiazhuang has increased significantly, and the accompanying emergence of high temperatures has become increasingly serious. In this case, city managers should be more cautious in formulating policies and focus on the protection and adaptation of natural resources.

B. Limitations

This study examines the between LC change and LST distribution was studied through assessing the spatiotemporal characteristics of LC and LST. Distribution trend of vegetation cover and its correlation with LST were analyzed using NDVI. However, the association between LC and LST is multifaceted; other influencing factors were not analyzed in this study. The influence of precipitation, climate zones, and other factors should be further analyzed in the future. We can also organically combine the change in LC and the forecast of the heat island index to offer a useful reference for forthcoming urban planning.

VI. Conclusion

This study investigated the correlation between LC changes and UHI using qualitative and quantitative analyses. Considering Shijiazhuang city as the study object, the following conclusions were reached.

1) From 2004–2019, the area of built-up area increased noticeably (5.177%), accompanied by a large decline in cropland and grassland (−3.342% and −3.625%). The direction of urbanization was mainly north–south.
2) The distribution of LST in 2004 was concentrated in cryogenic regions. During the duration of the study period, the distribution of LST became more homogeneous, with its range moving toward warmer regions. The hot zone expands from the point distribution to the plane. The direction is the same as that of urbanization.
3) Barren areas had the highest average temperature, with built-up area following suit. Due to its extensive coverage, the built-up area emerges as the primary catalyst for the UHI phenomenon. Changes in the mean temperature resulting from water and forest LC had a significant cooling effect, whereas built-up areas and barren lands had the opposite effect. We must focus on the loss of forest and cropland due to the increase in barren land, as the effects of these changes on the climate are clear.
4) From 2004 to 2019, owing to urbanization, areas with high levels of NDVI decreased, whereas those with low levels of NDVI increased, and vegetated areas were replaced by heavily built-up areas, leading to a more serious UHI effect. The relationship between LST and NDVI was highly inverse. Urban growth is unavoidable, but the influence of the building area on UHI can be lessened by putting green plants in the right places.

UHI have several negative impacts on cities, encompassing elevated death rates, intensified heat conditions, and augmented levels of urban pollution. Many specific factors affect the temperature, such as pollution emissions and variations in heat absorption and transfer, as a consequence of changes in LC. However, the specific underlying mechanisms require additional research. Based on how the LC has changed in Shijiazhuang city during a 15-year period, the study shows how the appearance of UHI has changed and provides recommendations that can be used for urban planning.

Appendix

See Tables VII–IX.

TABLE IX
LST Differences Among Different LC From 2004 to 2019

Year	LST (°C)	Cropland	Forest	Grassland	Water	Barren	Built-up area
2004	MIN	20.379	15.883	19.877	22.632	24.960	23.637
	MAX	44.882	37.855	44.882	39.646	44.882	47.013
	MEAN	29.218	26.790	29.918	26.402	39.222	32.303
	STDEV	1.264	1.877	2.135	1.088	3.045	2.291
2010	MIN	18.897	11.162	11.748	23.240	27.399	24.252
	MAX	47.072	43.051	47.102	41.192	43.896	51.520
	MEAN	30.844	28.738	31.938	27.549	37.056	34.347
	STDEV	1.454	2.505	2.325	2.019	2.706	2.402
2015	MIN	21.747	12.486	21.160	25.895	30.965	26.971
	MAX	52.417	47.873	48.853	45.627	46.461	54.292
	MEAN	32.894	32.513	36.179	30.921	39.538	36.773
	STDEV	2.524	2.709	2.361	2.235	2.555	2.532
2019	MIN	9.215	9.215	9.215	9.215	31.606	9.215
	MAX	58.254	47.324	48.431	46.587	49.338	63.822
	MEAN	33.880	33.412	36.301	31.558	38.137	37.409
	STDEV	3.477	3.931	2.449	3.325	2.043	2.939

REFERENCES

[1] M. Chen, H. Zhang, W. Liu, and W. Zhang, "The global pattern of urbanization and economic growth: Evidence from the last three decades," *PLoS One*, vol. 9, no. 8, Aug. 2014, Art. no. e103799, doi: 10.1371/journal.pone.0103799.

[2] A. Alam, M. S. Bhat, and M. Maheen, "Using Landsat satellite data for assessing the land use and land cover change in Kashmir valley," *GeoJournal*, vol. 85, no. 6, pp. 1529–1543, Dec. 2020, doi: 10.1007/s10708-019-10037-x.

[3] D. Sun, C. Hu, Y. Wang, Z. Wang, and J. Zhang, "Examining spatio-temporal characteristics of urban heat islands and factors driving them in Hangzhou, China," *IEEE J. Sel. Topics Appl. Earth Observ. Remote Sens.*, vol. 14, pp. 8316–8325, 2021, doi: 10.1109/JSTARS.2021.3105586.

[4] J. A. Voogt and T. R. Oke, "Thermal remote sensing of urban climates," *Remote Sens. Environ.*, vol. 86, no. 3, pp. 370–384, Aug. 2003, doi: 10.1016/S0034-4257(03)00079-8.

[5] N. S. Mohammad Harmay, D. Kim, and M. Choi, "Urban heat island associated with land use/land cover and climate variations in Melbourne, Australia," *Sustain. Cities Soc.*, vol. 69, Jun. 2021, Art. no. 102861, doi: 10.1016/j.scs.2021.102861.

[6] T. R. Oke, "City size and the urban heat island," *Atmospheric Environ.*, vol. 7, pp. 769–779, Aug. 1973, doi: 10.1016/0004-6981(73)90140-6.

[7] I. D. Stewart, T. R. Oke, and E. S. Krayenhoff, "Evaluation of the 'local climate zone' scheme using temperature observations and model simulations," *Int. J. Climatol.*, vol. 34, no. 4, pp. 1062–1080, Mar. 2014, doi: 10.1002/joc.3746.

[8] B. Feizizadeh and T. Blaschke, "Examining urban heat island relations to land use and air pollution: Multiple endmember spectral mixture analysis for thermal remote sensing," *IEEE J. Sel. Topics Appl. Earth Observ. Remote Sens.*, vol. 6, no. 3, pp. 1749–1756, Jun. 2013, doi: 10.1109/JSTARS.2013.2263425.

[9] L. Georgeson, M. Maslin, M. Poessinouw, and S. Howard, "Adaptation responses to climate change differ between global megacities," *Nature Climate Change*, vol. 6, no. 6, pp. 584–588, Jun. 2016, doi: 10.1038/nclimate2944.

[10] N. B. Grimm et al., "Global change and the ecology of cities," *Science*, vol. 319, no. 5864, pp. 756–760, Feb. 2008, doi: 10.1126/science.1150195.

[11] T. Qiu, C. Song, Y. Zhang, H. Liu, and J. M. Vose, "Urbanization and climate change jointly shift land surface phenology in the northern mid-latitude large cities," *Remote Sens. Environ.*, vol. 236, Jan. 2020, Art. no. 111477, doi: 10.1016/j.rse.2019.111477.

[12] Y. Sun, X. Zhang, G. Ren, F. W. Zwiers, and T. Hu, "Contribution of urbanization to warming in China," *Nature Climate Change*, vol. 6, no. 7, pp. 706–709, Jul. 2016, doi: 10.1038/nclimate2956.

[13] J. Yang, Y. Wang, X. Xiao, C. Jin, J. (Cecilia) Xia, and X. Li, "Spatial differentiation of urban wind and thermal environment in different grid sizes," *Urban Climate*, vol. 28, Jun. 2019, Art. no. 100458, doi: 10.1016/j.uclim.2019.100458.

[14] L. Zhao et al., "Interactions between urban heat islands and heat waves," *Environ. Res. Lett.*, vol. 13, no. 3, Mar. 2018, Art. no. 034003, doi: 10.1088/1748-9326/aa9f73.

[15] B. Stone, "Urban and rural temperature trends in proximity to large US cities: 1951–2000," *Int. J. Climatol.*, vol. 27, no. 13, pp. 1801–1807, Nov. 2007, doi: 10.1002/joc.1555.

[16] M. L. Imhoff, P. Zhang, R. E. Wolfe, and L. Bounoua, "Remote sensing of the urban heat island effect across biomes in the continental USA," *Remote Sens. Environ.*, vol. 114, no. 3, pp. 504–513, Mar. 2010, doi: 10.1016/j.rse.2009.10.008.

[17] K. Li, Y. Chen, M. Wang, and A. Gong, "Spatial-temporal variations of surface urban heat island intensity induced by different definitions of rural extents in China," *Sci. Total Environ.*, vol. 669, pp. 229–247, Jun. 2019, doi: 10.1016/j.scitotenv.2019.03.100.

[18] S. D. Yabo et al., "Impact of land cover transformation on urban heat islands in Harbin, China," *Environ. Monit. Assessment*, vol. 194, no. 6, Jun. 2022, Art. no. 453, doi: 10.1007/s10661-022-10066-z.

[19] N. Clinton and P. Gong, "MODIS detected surface urban heat islands and sinks: Global locations and controls," *Remote Sens. Environ.*, vol. 134, pp. 294–304, Jul. 2013, doi: 10.1016/j.rse.2013.03.008.

[20] B. Tu, X. Liao, Q. Li, Y. Peng, and A. Plaza, "Local semantic feature aggregation-based transformer for hyperspectral image classification," *IEEE Trans. Geosci. Remote Sens.*, vol. 60, 2022, Art. no. 5536115, doi: 10.1109/TGRS.2022.3201145.

[21] B. Tu, X. Yang, W. He, J. Li, and A. Plaza, "Hyperspectral anomaly detection using reconstruction fusion of quaternion frequency domain analysis," *IEEE Trans. Neural Netw. Learn. Syst.*, early access, Jan. 31, 2023, doi: 10.1109/TNNLS.2022.3227167.

[22] B. Tu, X. Yang, X. Ou, G. Zhang, J. Li, and A. Plaza, "Ensemble entropy metric for hyperspectral anomaly detection," *IEEE Trans. Geosci. Remote Sens.*, vol. 60, 2022, Art. no. 5513617, doi: 10.1109/TGRS.2021.3116681.

[23] G. Dall'Olmo and A. Karnieli, "Monitoring phenological cycles of desert ecosystems using NDVI and LST data derived from NOAA-AVHRR imagery," *Int. J. Remote Sens.*, vol. 23, no. 19, pp. 4055–4071, Jan. 2002, doi: 10.1080/01431160110115988.

[24] Z. Qin and A. Karnieli, "Progress in the remote sensing of land surface temperature and ground emissivity using NOAA-AVHRR data," *Int. J. Remote Sens.*, vol. 20, no. 12, pp. 2367–2393, Jan. 1999, doi: 10.1080/014311699212074.

[25] M. Stathopoulou and C. Cartalis, "Downscaling AVHRR land surface temperatures for improved surface urban heat island intensity estimation," *Remote Sens. Environ.*, vol. 113, no. 12, pp. 2592–2605, Dec. 2009, doi: 10.1016/j.rse.2009.07.017.

[26] Z. Wang, Z. Lu, and G. Cui, "Spatiotemporal variation of land surface temperature and vegetation in response to climate change based on NOAA-AVHRR data over China," *Sustainability*, vol. 12, no. 9, Apr. 2020, Art. no. 3601, doi: 10.3390/su12093601.

[27] K. Liu, H. Su, X. Li, W. Wang, L. Yang, and H. Liang, "Quantifying spatial–temporal pattern of urban heat island in beijing: An improved assessment using land surface temperature (LST) time series observations from LANDSAT, MODIS, and Chinese new satellite GaoFen-1," *IEEE J. Sel. Topics Appl. Earth Observ. Remote Sensin*, vol. 9, no. 5, pp. 2028–2042, May 2016, doi: 10.1109/JSTARS.2015.2513598.

[28] W. Zhao, J. He, Y. Wu, D. Xiong, F. Wen, and A. Li, "An analysis of land surface temperature trends in the central Himalayan region based on MODIS products," *Remote Sens.*, vol. 11, no. 8, Apr. 2019, Art. no. 900, doi: 10.3390/rs11080900.

[29] A. Jia, H. Ma, S. Liang, and D. Wang, "Cloudy-sky land surface temperature from VIIRS and MODIS satellite data using a surface energy balance-based method," *Remote Sens. Environ.*, vol. 263, Sep. 2021, Art. no. 112566, doi: 10.1016/j.rse.2021.112566.

[30] F. Zhang et al., "Cloud-free land surface temperature reconstructions based on MODIS measurements and numerical simulations for characterizing surface urban heat islands," *IEEE J. Sel. Topics Appl. Earth Observ. Remote Sens.*, vol. 15, pp. 6882–6898, Aug. 2022, doi: 10.1109/JSTARS.2022.3199248.

[31] W. Yu et al., "Attribution of urban diurnal thermal environmental change: Importance of global–local effects," *IEEE J. Sel. Topics Appl. Earth Observ. Remote Sens.*, vol. 16, pp. 8087–8101, Aug. 2023, doi: 10.1109/JSTARS.2023.3308045.

[32] J. A. Sobrino, R. Oltra-Carrió, G. Sòria, R. Bianchi, and M. Paganini, "Impact of spatial resolution and satellite overpass time on evaluation of the surface urban heat island effects," *Remote Sens. Environ.*, vol. 117, pp. 50–56, Feb. 2012, doi: 10.1016/j.rse.2011.04.042.

[33] H. Chen, Q. Deng, Z. Zhou, Z. Ren, and X. Shan, "Influence of land cover change on spatio-temporal distribution of urban heat island —A case in Wuhan main urban area," *Sustain. Cities Soc.*, vol. 79, Apr. 2022, Art. no. 103715, doi: 10.1016/j.scs.2022.103715.

[34] X. Yu, X. Guo, and Z. Wu, "Land surface temperature retrieval from landsat 8 TIRS—Comparison between radiative transfer equation-based method, split window algorithm and single channel method," *Remote Sens.*, vol. 6, no. 10, pp. 9829–9852, Oct. 2014, doi: 10.3390/rs6109829.

[35] D. Choudhury, K. Das, and A. Das, "Assessment of land use land cover changes and its impact on variations of land surface temperature in Asansol-Durgapur development region," *Egyptian J. Remote Sens. Space Sci.*, vol. 22, no. 2, pp. 203–218, Aug. 2019, doi: 10.1016/j.ejrs.2018.05.004.

[36] M. Mohan and A. Kandya, "Impact of urbanization and land-use/land-cover change on diurnal temperature range: A case study of tropical urban airshed of India using remote sensing data," *Sci. Total Environ.*, vol. 506–507, pp. 453–465, Feb. 2015, doi: 10.1016/j.scitotenv.2014.11.006.

[37] H. Feng, X. Zhao, F. Chen, and L. Wu, "Using land use change trajectories to quantify the effects of urbanization on urban heat island," *Adv. Space Res.*, vol. 53, no. 3, pp. 463–473, 2014, doi: 10.1016/j.asr.2013.11.028.

[38] R. Amiri, Q. Weng, A. Alimohammadi, and S. K. Alavipanah, "Spatial–temporal dynamics of land surface temperature in relation to fractional vegetation cover and land use/cover in the Tabriz urban area, Iran," *Remote Sens. Environ.*, vol. 113, no. 12, pp. 2606–2617, Dec. 2009, doi: 10.1016/j.rse.2009.07.021.

[39] H. Xu, F. Ding, and X. Wen, "Urban expansion and heat island dynamics in the quanzhou region, China," *IEEE J. Sel. Topics Appl. Earth Observ. Remote Sens.*, vol. 2, no. 2, pp. 74–79, Jun. 2009, doi: 10.1109/JSTARS.2009.2023088.

[40] Q. Weng, D. Lu, and J. Schubring, "Estimation of land surface temperature-vegetation abundance relationship for urban heat island studies," *Remote Sens. Environ.*, vol. 89, no. 4, pp. 467–483, 2004, doi: 10.1016/j.rse.2003.11.005.

[41] K. J. Gohain, P. Mohammad, and A. Goswami, "Assessing the impact of land use land cover changes on land surface temperature over Pune city, India," *Quaternary Int.*, vol. 575–576, pp. 259–269, Feb. 2021, doi: 10.1016/j.quaint.2020.04.052.

[42] S. Pal and S. Ziaul, "Detection of land use and land cover change and land surface temperature in English Bazar urban centre," *Egyptian J. Remote Sens. Space Sci.*, vol. 20, no. 1, pp. 125–145, Jun. 2017, doi: 10.1016/j.ejrs.2016.11.003.

[43] Y. Zhang, H. Balzter, B. Liu, and Y. Chen, "Analyzing the impacts of urbanization and seasonal variation on land surface temperature based on subpixel fractional covers using landsat images," *IEEE J. Sel. Topics Appl. Earth Observ. Remote Sens.*, vol. 10, no. 4, pp. 1344–1356, Apr. 2017, doi: 10.1109/JSTARS.2016.2608390.

[44] S. C. Sam and G. Balasubramanian, "Spatiotemporal detection of land use/land cover changes and land surface temperature using Landsat and MODIS data across the coastal Kanyakumari district, India," *Geodesy Geodynamics*, vol. 14, no. 2, pp. 172–181, Mar. 2023, doi: 10.1016/j.geog.2022.09.002.

[45] J. Xin, J. Yang, D. Sun, T. Han, C. Song, and Z. Shi, "Seasonal differences in land surface temperature under different land use/land cover types from the perspective of different climate zones," *Land*, vol. 11, no. 8, Jul. 2022, Art. no. 1122, doi: 10.3390/land11081122.

[46] X. Geng, Z. Yu, D. Zhang, C. Li, Y. Yuan, and X. Wang, "The influence of local background climate on the dominant factors and threshold-size of the cooling effect of urban parks," *Sci. Total Environ.*, vol. 823, Jun. 2022, Art. no. 153806, doi: 10.1016/j.scitotenv.2022.153806.

[47] J. Yang and X. Huang, "The 30 m annual land cover datasets and its dynamics in China from 1985 to 2022," *Earth Syst. Sci. Data*, vol. 13, no. 1, pp. 3907–3925, Aug. 2023, doi: 10.5281/zenodo.8176941.

[48] A. R. Huete and H. Q. Liu, "An error and sensitivity analysis of the atmospheric- and soil-correcting variants of the NDVI for the MODIS-EOS," *IEEE Trans. Geosci. Remote Sens.*, vol. 32, no. 4, pp. 897–905, Jul. 1994, doi: 10.1109/36.298018.

[49] C. Leprieur, Y. H. Kerr, S. Mastorchio, and J. C. Meunier, "Monitoring vegetation cover across semi-arid regions: Comparison of remote observations from various scales," *Int. J. Remote Sens.*, vol. 21, no. 2, pp. 281–300, Jan. 2000, doi: 10.1080/014311600210830.

[50] Y. Julien and J. A. Sobrino, "The yearly land cover dynamics (YLCD) method: An analysis of global vegetation from NDVI and LST parameters," *Remote Sens. Environ.*, vol. 113, no. 2, pp. 329–334, Feb. 2009, doi: 10.1016/j.rse.2008.09.016.

[51] G. Grigoraș and B. Urițescu, "Land use/land cover changes dynamics and their effects on surface urban heat island in bucharest, Romania," *Int. J. Appl. Earth Observation Geoinf.*, vol. 80, pp. 115–126, Aug. 2019, doi: 10.1016/j.jag.2019.03.009.

[52] Q.-V. Doan and H. Kusaka, "Numerical study on regional climate change due to the rapid urbanization of greater Ho Chi Minh City's metropolitan area over the past 20 years," *Int. J. Climatol.*, vol. 36, no. 10, pp. 3633–3650, Aug. 2016, doi: 10.1002/joc.4582.

[53] P. Si, Y. Ren, D. Liang, and B. Lin, "The combined influence of background climate and urbanization on the regional warming in Southeast China," *J. Geographical Sci.*, vol. 22, no. 2, pp. 245–260, Apr. 2012, doi: 10.1007/s11442-012-0924-3.

[54] X. Yao, Z. Wang, and H. Wang, "Impact of urbanization and land-use change on surface climate in middle and lower reaches of the Yangtze River, 1988–2008," *Adv. Meteorol.*, vol. 2015, pp. 1–10, 2015, doi: 10.1155/2015/395094.

[55] D. Zhou, S. Zhao, L. Zhang, G. Sun, and Y. Liu, "The footprint of urban heat island effect in China," *Sci. Rep.*, vol. 5, no. 1, Jun. 2015, Art. no. 11160, doi: 10.1038/srep11160.

[56] L. Bounoua et al., "Impact of urbanization on US surface climate," *Environ. Res. Lett.*, vol. 10, no. 8, Aug. 2015, Art. no. 084010, doi: 10.1088/1748-9326/10/8/084010.

[57] W. Liao et al., "Stronger contributions of urbanization to heat wave trends in wet climates," *Geophysical Res. Lett.*, vol. 45, no. 20, pp. 11310–11317, Oct. 2018, doi: 10.1029/2018GL079679.

[58] J. M. Shepherd, "Evidence of urban-induced precipitation variability in arid climate regimes," *J. Arid Environments*, vol. 67, no. 4, pp. 607–628, Dec. 2006, doi: 10.1016/j.jaridenv.2006.03.022.

[59] A. Grover and R. Singh, "Analysis of urban heat island (UHI) in relation to normalized difference vegetation index (NDVI): A comparative study of Delhi and Mumbai," *Environments*, vol. 2, no. 4, pp. 125–138, Apr. 2015, doi: 10.3390/environments2020125.

[60] J. Li, C. Song, L. Cao, F. Zhu, X. Meng, and J. Wu, "Impacts of landscape structure on surface urban heat islands: A case study of Shanghai, China," *Remote Sens. Environ.*, vol. 115, no. 12, pp. 3249–3263, Dec. 2011, doi: 10.1016/j.rse.2011.07.008.

Linxue Tian is currently working toward the master's degree in cartography and geographic information systems with Liaoning Normal University, Dalian, China.

Her current research interests include urban thermal infrared remote sensing, urban space growth, and urban ventilation.

Jun Yang received the Ph.D. degree in human geography from Liaoning Normal University, Dalian, China, in 2009.

He is currently a Professor with the Jangho Architecture College and School of Humanities and Law in Northeastern University, Shenyang, China. He is also with Liaoning Normal University, Dalian, China, working on the effect of human settlement and GIS. His research interests include urban space growth urban thermal environmental, cellular automata land-use change, and urban human settlements, as well as other aspects of research.

Cui Jin received the Ph.D. degree in geographic information science from the University of Oklahoma, Norman, OK, USA, in 2016.

She is currently an Associate Professor with the School of Geographical Sciences, Liaoning Normal University, Dalian, China. Her research interests include the field of global climate change remote sensing, vegetation carbon cycling remote sensing, agricultural remote sensing, and land-use and land-cover change research.